

Supplementary Information

Sustainable p-type copper selenide solar material with ultra-large absorption coefficient

Erica M. Chen¹, Logan Williams¹, Alan Olvera¹, Cheng Zhang², Mingfei Zhang¹, Guangsha Shi¹, John T. Heron¹, Liang Qi¹, L. Jay Guo², Emmanouil Kioupakis¹, and Pierre F. P. Poudeu^{1*}

¹Department of Materials Science and Engineering, University of Michigan, Ann Arbor, 48109, USA

²Department of Electrical Engineering & Computer Science, University of Michigan, Ann Arbor 48109, USA

Content:

Tables S1 to S3

Figures S1 to S9

Table S1: Selected crystallographic data for Cu₄TiSe₄ at 300 K

| | |
|--|---|
| Crystal system; space group | F-43c; (No. 219) |
| Formula weight (g/mol) | 1235.8 |
| Density (ρ_{cal}) (g/cm ³) | 5.69815 |
| Lattice parameter (Å) $a = b = c$ | 11.2936(13) |
| Volume (Å ³); Z | 1440.45(29); 4 |
| Crystal size (mm) | [0.05] x [0.05] x [0.05] |
| Crystal shape, color | Faceted cubic, dark gray |
| Radiation (Å) | $\lambda(\text{MoK}\alpha) = 0.71073$ |
| μ (cm ⁻¹) | 327.8 |
| Diff. electron density (e/ Å ³) | +2.20 to -1.78 |
| Transmission factor | 0.2997 – 0.6709 |
| 2range; index range | $6.2^\circ \leq 2\theta \leq 59.80^\circ$; $-15 \leq h \leq 15$; $-15 \leq k \leq 15$; $-14 \leq l \leq 15$ |
| R_1 ($F_o > 4\sigma(F_o)$) ^a | 0.0414 |
| wR_2 (all) ^b | 0.1025 |
| Goodness of fit | 1.030 |

^[a] $R_1 = \sum ||F_o| - |F_c|| / \sum |F_o|$; ^[b] $wR_2 = [\sum w(F_o^2 - F_c^2)^2 / \sum w(F_o^2)^2]^{1/2}$

Table S2: Atomic coordinates, Wyckoff positions (W. P.), site occupancy factors, and equivalent isotropic displacement parameters (U_{eq} in \AA^2) for all atoms in CTiSe

| Atom | W.P. | S. O. F. | x | y | z | U_{eq} |
|------|------|----------|------------|------------|------------|-----------------|
| Se1 | 32e | 0.33333 | 0.12432(8) | 0.12432(8) | 0.12432(8) | 0.01274 |
| Cu2 | 24d | 0.25000 | 1/4 | 0 | 0 | 0.01536 |
| Cu1 | 8a | 0.08333 | 0 | 0 | 0 | 0.02828 |
| Ti1 | 8b | 0.08333 | 1/4 | 1/4 | 1/4 | 0.04238 |

U_{eq} is defined as one-third of the trace of the orthogonalized U_{ij} tensor.

Table S3: Selected inter-atomic distances (\AA) in CTiSe

| Bond Type | Bond Distance (\AA) |
|-----------------------------------|--------------------------------|
| Cu2-Se1 ^{iii, iv, v} | 2.4407(6) |
| Cu1-Se1 ^{iii, vii, viii} | 2.4318(2) |
| Ti1-Se1 ^{xi, xii, xiii} | 2.4584(2) |

Operators for generating equivalent atoms:

(i) y, z, x ; (ii) z, x, y ; (iii) $x, -y, -z$; (iv) $0.5-y, x, -z$; (v) $0.5-y, -x, z$; (vi) $0.5+y, x, z$; (vii) $-x, y, -z$; (viii) $-x, -y, z$; (ix) $-y, z, -x$; (x) $z, -x, -y$; (xi) $x, 0.5-y, 0.5-z$; (xii) $0.5-x, 0.5-y, z$; (xiii) $0.5-x, y, 0.5-z$.

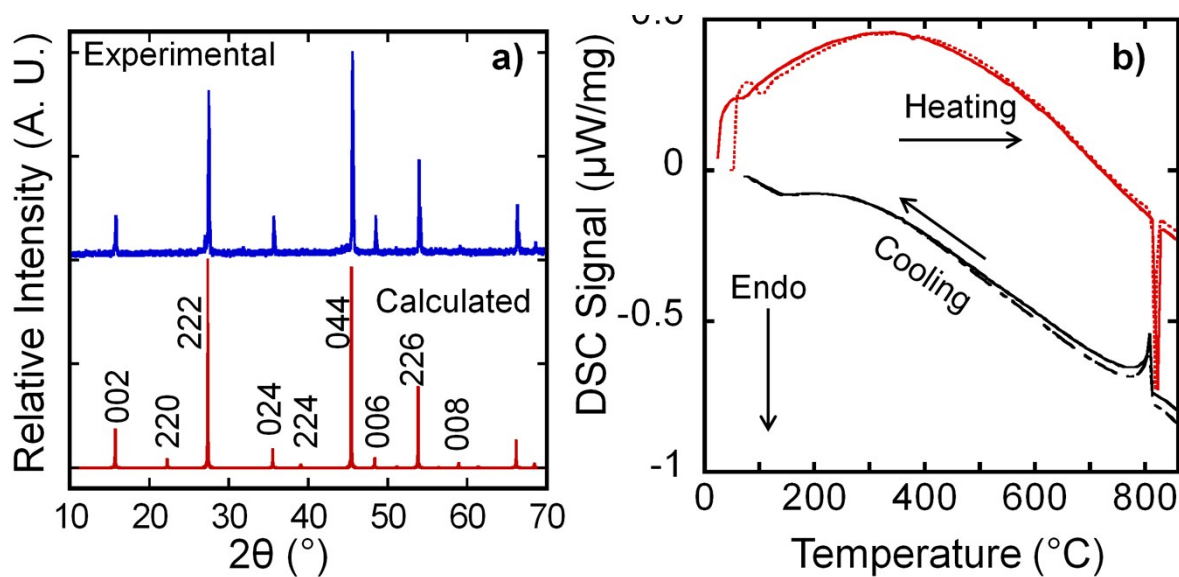


Figure S1: a) Powered X-ray diffraction of the synthesized polycrystalline powder of CTSe compared to theoretical pattern calculated using single crystal data. The excellent matching in both peak position and relative intensity indicates successful synthesis of single-phase powder of CTSe. b) Differential scanning calorimetry (DSC) heating and cooling curves for CTSe. The reproducibility of DSC signals on both heating and cooling curves indicates the thermal stability of the compound.

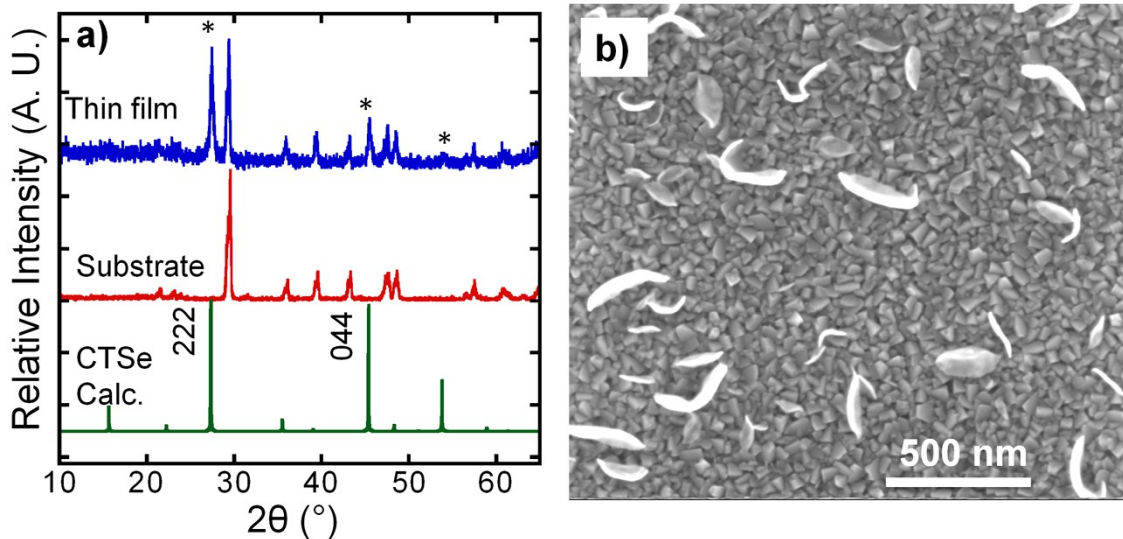


Figure S2: a) Powder X-ray diffraction patterns of PLD-deposited CTSe film compared to the X-ray diffraction pattern of the bare substrate and the theoretical pattern calculated from single crystal data. The asterisks (*) indicate peaks from CTSe. b) Scanning electron microscopy (SEM) image of CTSe film deposited using PLD, revealing the uniform grain size and morphology. The white flakes on SEM image are large particles of CTSe chipped out of the target.

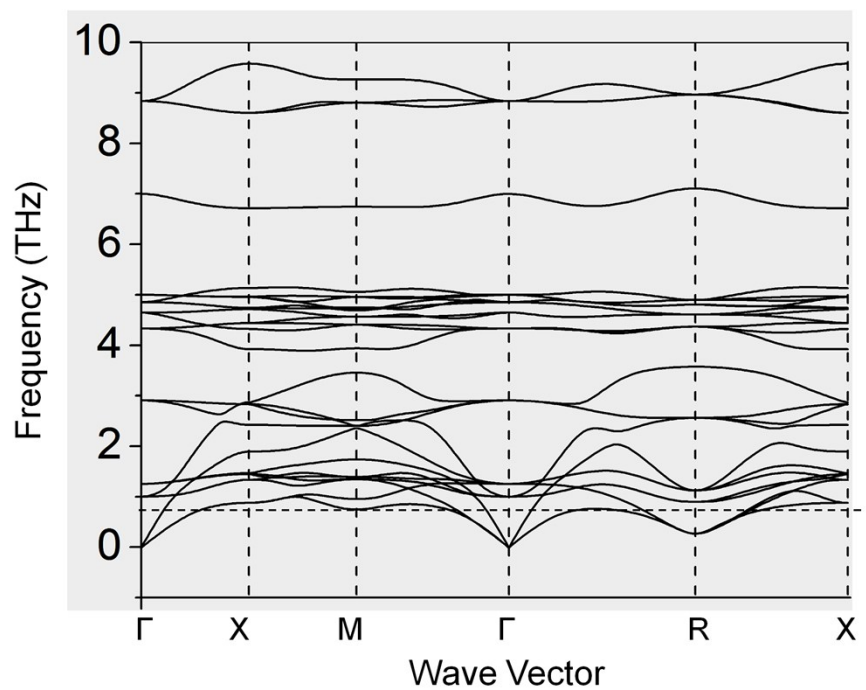


Figure S3: Calculated phonon dispersion relation of CTSe. No negative phonon frequencies are observed throughout the Brillouin zone, indicating the dynamic stability of CTSe upon small inhomogeneous deformation.

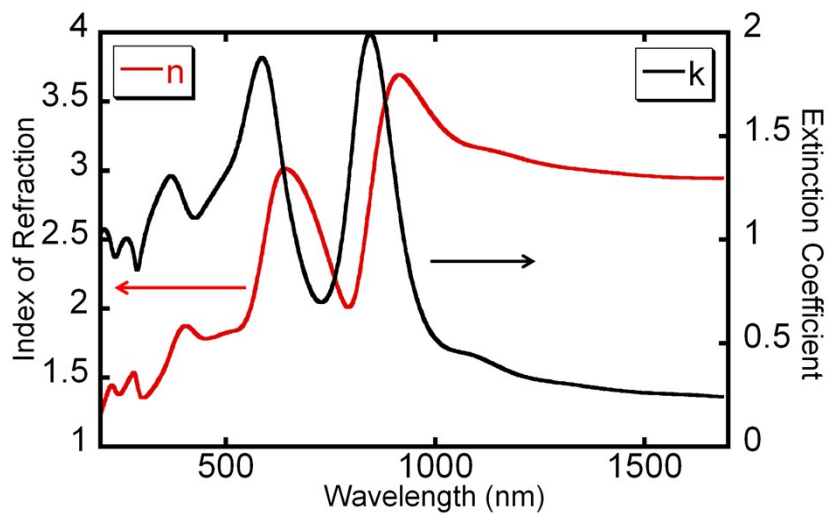


Figure S4: Index of refraction (n) and the extinction coefficient (k) as a function of wavelength extracted from ellipsometry data.

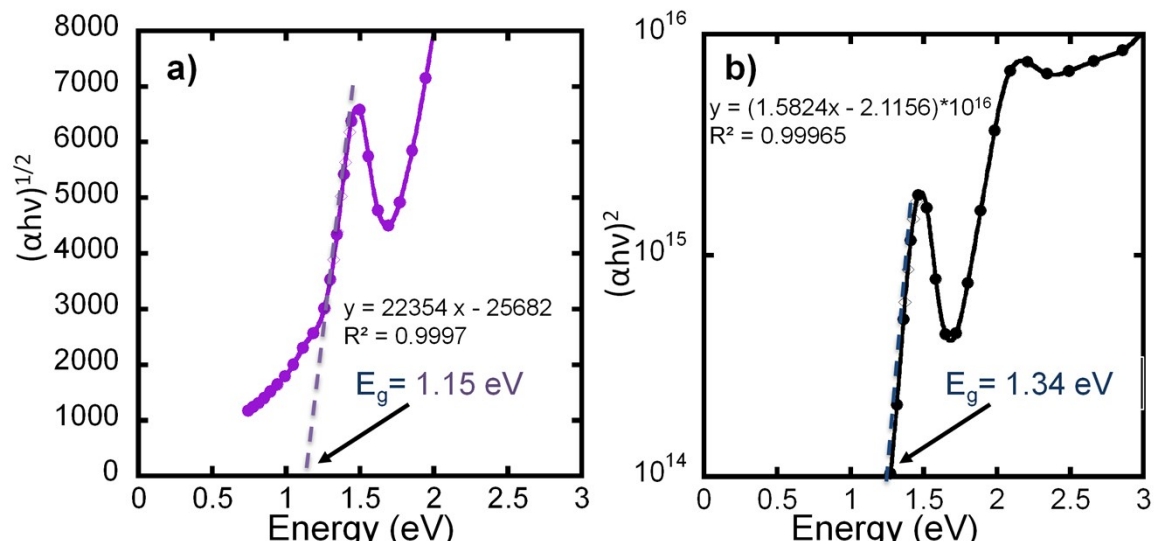


Figure S5: Tauc analysis for the determination of optical band gap. a) allowed indirect transition and b) allowed direct transition.

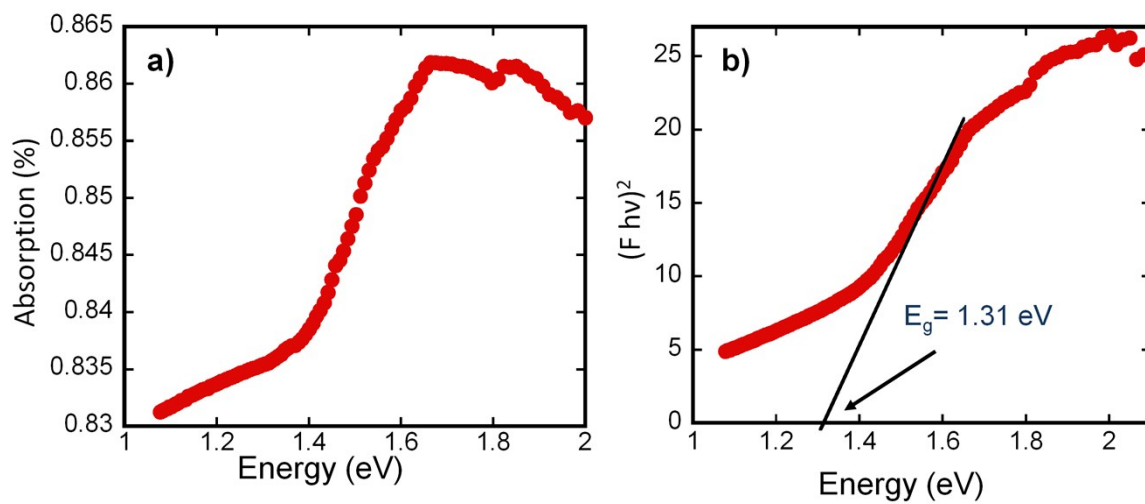


Figure S6: (a) Diffuse reflectance data on bulk CTSe powder. (b) Tauc fitting for allowed direct transition using diffuse reflectance data indicating an optical band gap of $\sim 1.31 \text{ eV}$.

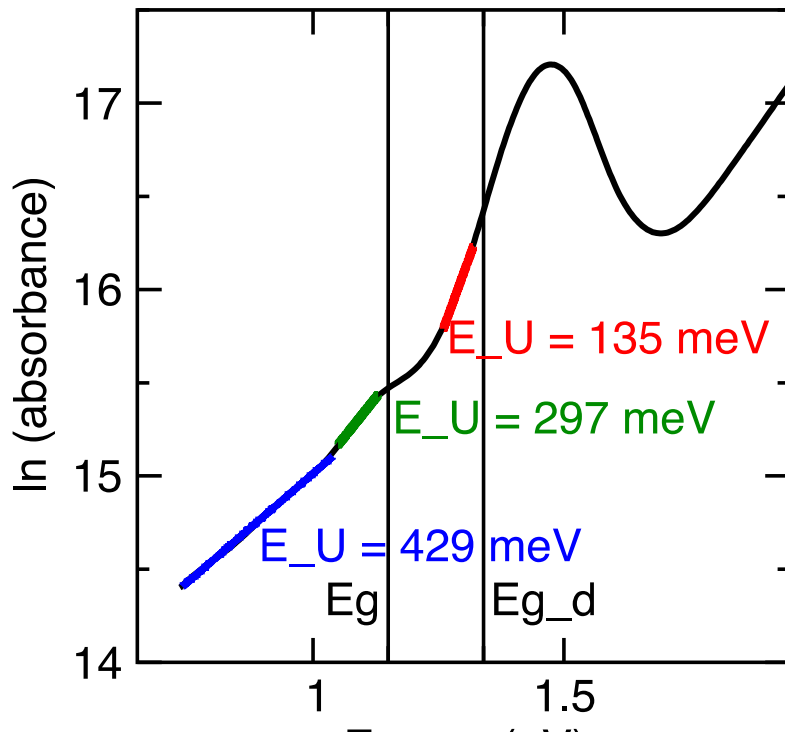


Figure S7: Urbach tail analysis of the optical absorbance of CTSe. The Urbach energy is calculated using the empirical formula $\ln\alpha = \ln\alpha_0 + (h\nu/E_U)$ and fitting the linear region of $\ln\alpha$ vs $h\nu$. Urbach absorption tails typically arise from thermal fluctuation at the band edges or the presence of defects. Three linear regions are present giving Urbach energy (E_U) of 135 meV, 297 meV, and 429 meV within CTSe band gap. The large values obtained for the Urbach energy point to large concentrations of defects existing within the band gap.

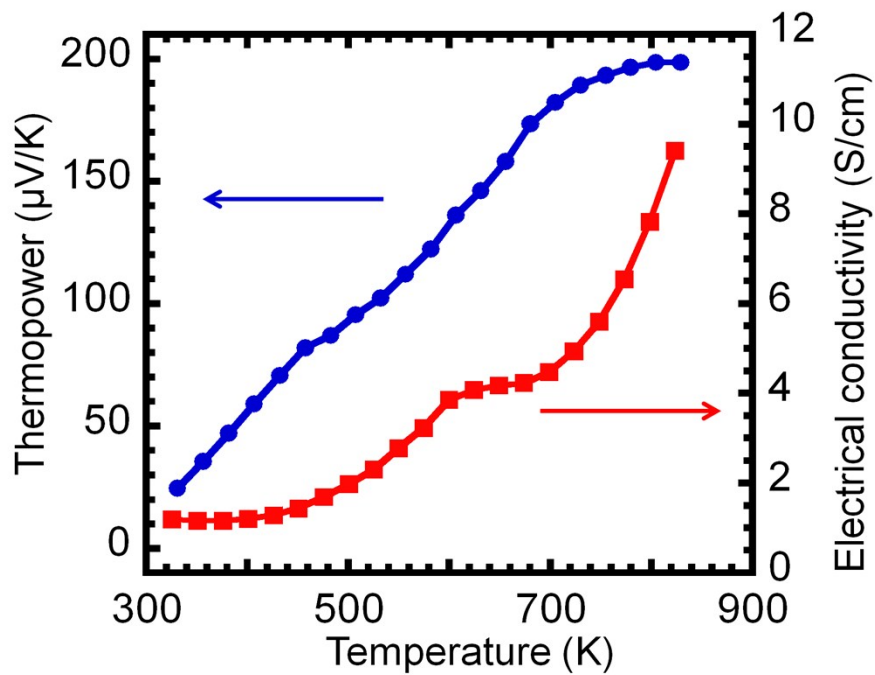


Figure S8: Temperature dependence of the thermopower (S) and electrical conductivity (σ) of CTSe. The positive values of the thermopower indicate holes as the majority carriers and the gradual increase of the electrical conductivity with rising temperature is consistent with the intrinsic semiconducting behavior of the compound.

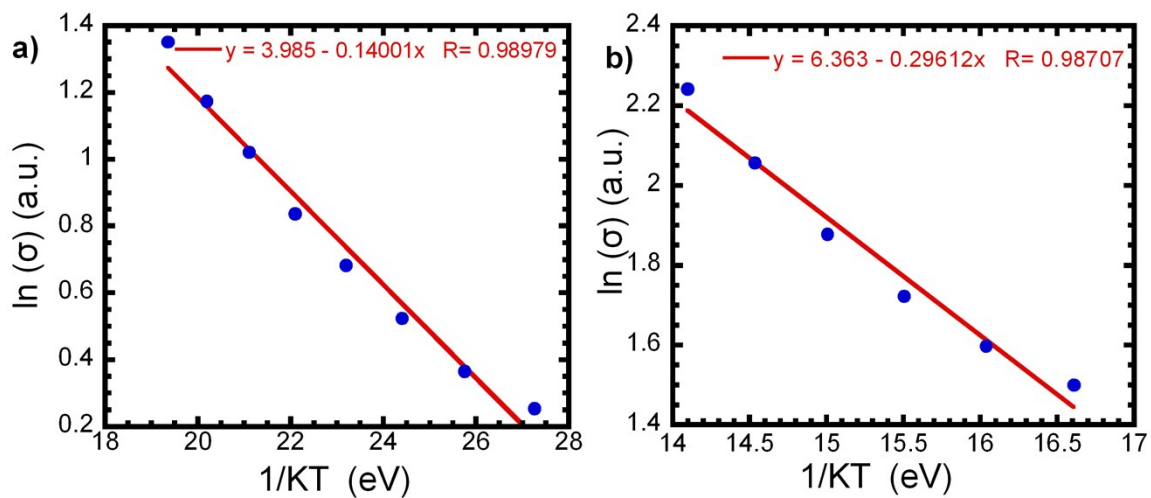


Figure S9: Fitting of the electrical conductivity of CTSe using Arrhenius equation for thermal activation conductivity, $\text{Ln}(\sigma) = \text{Ln}(\sigma_0) - E_a/KT$. (a) low temperature transition (400 to 600 K) with activation energy of ~ 140 meV; (b) high temperature transition (700 to 800 K) with activation energy of ~ 296 meV.